

Influence of the atomic modeling on the electron capture process

X. Mougeot,^{1, a} L. Mouawad,² A. Andoche,² and P.-A. Hervieux^{2, b}

¹*Université Paris-Saclay, CEA, List,
Laboratoire National Henri Becquerel (LNE-LNHB), F-91120 Palaiseau, France*

²*Université de Strasbourg, CNRS, Institut de
Physique et Chimie des Matériaux de Strasbourg,
UMR 7504, F-67000 Strasbourg, France*

(Dated: December 1, 2021)

Abstract

Ongoing experimental efforts to measure with unprecedented precision electron capture probabilities will challenge the current theoretical models. The short range of the weak interaction necessitates an accurate description of the atomic structure down to the nucleus region. In this study, an atomic modeling has been developed in the framework of the relativistic density functional theory within which several exchange-correlation functionals and self-interaction-corrected models have been explored. A recent electron capture model has been modified in order to only test the influence of the atomic modeling on the calculated decay probabilities. In particular, two important possibilities have been tested, the “no vacancy” and the “frozen orbital” approximations. Results have been compared to experimental values evaluated from available published data. New high-precision measurements are strongly encouraged as the accuracy of the current experimental values does not allow to draw a firm conclusion on the theoretical modeling to be employed.

arXiv:2111.15321v1 [physics.atom-ph] 30 Nov 2021

^a xavier.mougeot@cea.fr

^b hervieux@unistra.fr

I. Introduction

Electron capture is a low-energy weak interaction process in which a proton embedded in a nucleus absorbs an atomic electron, leading to a nucleus of a lower atomic number and the emission of a neutrino with a well-defined energy. If the daughter nucleus is not in its ground state after the transition, its deexcitation goes through a cascade of γ transitions that leads to the emission of either γ -rays or internal conversion electrons, the latter creating atomic vacancies. In addition, the daughter atom just after the transition is overall neutral but in an excited state, the capture process being seen in its electronic configuration as the promotion of the captured electron to the valence shell. The subsequent relaxation of the daughter atom then leads to the emission of X-rays and Auger electrons all along the propagation of the vacancies, until their final disappearance.

Ground-state to ground-state transitions are very difficult to measure, especially for low-mass nuclei, because only X-rays and Auger electrons of very low energies can be detected. Standardization of such pure electron capture emitters in radionuclide metrology is challenging and directly depends on the knowledge of the capture probabilities, which most often come from theory. Recently, a new international reference system, called ESIR [1], has been established by the International Bureau of Weights and Measures (BIPM) based on activity measurements carried out with the liquid scintillation counting (LSC) technique. The computed LSC efficiency strongly decreases at very low energy and a precise modeling of the atomic rearrangement is necessary, which depends on the number of initial vacancies [2].

What is problematic for radionuclide metrology can become an advantage in nuclear medicine for cancer treatment when the radioactive nuclei are correctly vectorized into the human body. The vast majority of Auger electrons are emitted with a few keV kinetic energy, deposited in a range from nanometers to micrometers. This property makes them highly promising for an accurate, well-controlled internal radiotherapy at the cell or even the DNA level. Many short-lived nuclei decaying by electron capture have been studied in this perspective [3,4].

Long-lived isotopes can also be useful in other contexts. The decommissioning of legacy nuclear sites necessitates the radioactivity inventory of various materials. When non-destructive techniques such as γ spectrometry are impossible, precise measurements of samples are used together with scaling methods to estimate the total amount of radioactivity [5,6]. Some long-lived pure electron capture emitters have been used to investigate the age of the Solar System [7,8] and the irradiation history of meteorites and lunar samples [9].

Every application refers to evaluated nuclear decay data, which can be taken either in the ENSDF (Evaluated Nuclear Structure Data File) database [10] or in the DDEP (Decay Data Evaluation Project) database [11], the latter being recommended by the BIPM for metrology purposes. In ENSDF evaluations, the properties of β transitions and electron captures are still calculated with the LogFT code [12], which is based on an approximate theoretical model limited by the computing power available in the 1970s. Recently, the BetaShape code has been developed by one of the authors in order to improve the theoretical predictions for β transitions and electron captures [13,14]. Its modeling takes into account several additional physical phenomena and provides much more detailed information required by different communities. The DDEP collaboration has already adopted this new code for its nuclear data evaluations.

Capture probabilities from BetaShape have been compared to a selection of measurements available in the literature, concluding to the need of new high-precision measurements to validate and constrain the theoretical models [15]. This is in part at the origin of the

European metrology project MetroMMC [16], which aims at improving the knowledge of electron capture decay and the subsequent atomic relaxation processes. The high-precision measurements from this project will challenge the theoretical predictions, for which the accuracy of the atomic modeling is pivotal.

Indeed, as the electron capture process takes place inside the nucleus, it is mandatory to develop models that are as precise as possible and capable of describing the electronic properties of atoms in this space region. In addition, we can also wonder about the role played by electron correlations in the decay process. Trying to answer these two issues constitute the main goal of this work.

We first describe briefly the electron capture modeling and the determination of the atomic wave functions in the BetaShape code. Next, a model developed in the framework of relativistic density functional theory within the local density approximation (RLDA) is described in details. Within the latter, most popular exchange-correlation functionals and self-interaction-corrected models have been explored. Binding energies, wave functions and capture probabilities are finally compared between each other, and to experimental values when available.

II. Theoretical methods

Our modeling of electron capture decays is based on the formalism from [17,18] and has already been described in detail in [15,14]. In this section, we focus on the dependency of this modeling on the atomic wave functions, and on the determination of the wave functions themselves.

A. Electron capture

The low rest mass of the beta particle compared to the transition energies necessitates a fully relativistic formalism of electron capture decay, usually expressed in relativistic units ($\hbar = m_e = c = 1$). Considering spherical symmetry, radial and angular parts of the wave functions can be separated. An atomic orbital is then characterized by its quantum numbers (n, κ) , the latter being the eigenvalue of the operator $K = \beta(\vec{\sigma} \cdot \vec{L} + 1)$ defined from the Dirac (β) and Pauli ($\vec{\sigma}$) matrices and the angular momentum operator (\vec{L}).

Atomic levels being degenerated, one has to introduce their relative occupation number $n_{n\kappa}$. In addition, each wave function is characterized by its Coulomb amplitude $\beta_{n\kappa}$, as defined in [17,18]. This quantity has to be computed and resumes to the value of the wave function at the origin ($r = 0$) for $\kappa = -1$, i.e. in the case of $s_{1/2}$ orbitals (see Section III B).

The transition probability per unit of time can be derived by applying first-order time-dependent perturbation theory and results in the sum of the capture probability of each subshell:

$$\lambda_\varepsilon = \frac{G_\beta^2}{2\pi^3} \sum_{n,\kappa} \frac{\pi}{2} n_{n\kappa} C_{n\kappa} q_{n\kappa}^2 \beta_{n\kappa}^2 B_{n\kappa} \left(1 + \sum_{m,\kappa} P_{m\kappa} \right) \quad (1)$$

with G_β the Fermi coupling constant and $q_{n\kappa}$ the neutrino momentum. We do not consider in the present work any electron capture decay for which the available energy would be sufficient for a competition with a β^+ transition.

The quantity $C_{n\kappa}$ couples the lepton and nucleon wave functions. For allowed and forbidden unique transitions, the nuclear dependency acts as a constant factor. Therefore, determining ratios of relative capture probabilities prevents from introducing any nuclear

structure. In such cases,

$$C_{n\kappa} \propto \frac{p_{n\kappa}^{2(k-1)} q_{n\kappa}^{2(L-k)}}{(2k-1)![2(L-k)+1!]} \quad (2)$$

with $k = |\kappa|$, $p_{n\kappa}$ the electron momentum and $L = |J_i - J_f|$ the difference between the total angular momenta of initial and final nuclear levels.

The quantity $B_{n\kappa}$ is a correction that accounts for overlap and exchange effects. The former is induced by the capture process that changes the nucleus charge, leading to an imperfect overlap of the initial and final wave functions of the spectator electrons. The latter arises from electrons being identical particles. The two following methods, available in the literature, have been considered in the BetaShape code for calculating $B_{n\kappa}$. Bahcall's approach [19] only considers the first three $s_{1/2}$ orbitals, assumes a complete set of states for the other orbitals and makes use of the closure property to sum over the continuum states. Vatai's approach [20] considers in addition the exchange term of the $4s_{1/2}$ orbital and the overlap correction of each subshell, but does not use the closure property. The generalization of these approaches [15] leads to $B_{n\kappa} = |b_{n\kappa}/\beta_{n\kappa}|^2$ with

$$b_{n\kappa} = t_{n\kappa} \left[\prod_{m \neq n} \langle (m, \kappa)' | (m, \kappa) \rangle \right] \times \left[\beta_{n\kappa} - \sum_{m \neq n} \beta_{m\kappa} \frac{\langle (m, \kappa)' | (n, \kappa) \rangle}{\langle (m, \kappa)' | (m, \kappa) \rangle} \right], \quad (3)$$

where $\langle (m, \kappa)' | (m, \kappa) \rangle$ is the overlap of the atomic wave functions between the initial (m, κ) state and the final $(m, \kappa)'$ state, and correspondingly for the other overlaps. Bahcall's model is given by $t_{n\kappa} = 1$ and Vatai's model by

$$t_{n\kappa} = \langle (n, \kappa)' | (n, \kappa) \rangle^{n_{n\kappa}-1/2|\kappa|} \times \left[\prod_{m \neq n} \langle (m, \kappa)' | (m, \kappa) \rangle^{n_{m\kappa}-1} \right] \times \left[\prod_{\substack{m, \mu \\ \mu \neq \kappa}} \langle (m, \mu)' | (m, \mu) \rangle^{n_{m\mu}} \right]. \quad (4)$$

The difference between Bahcall and Vatai models in the resulting capture probabilities is used in BetaShape as a theoretical uncertainty component. The other component comes from input data and corresponds to the propagation of the uncertainty on the transition energy.

The last term in Equation (1) corrects for the shaking effects, i.e. internal excitation (shake-up) and internal ionization (shake-off). These effects take into account additional final states in which other atomic vacancies are present with the initial vacancy due to capture. The modeling implemented in BetaShape is limited to a single additional vacancy due to shaking. The separate calculation of each process requires the knowledge of all unoccupied bound states up to the Fermi level for shake-up, and summing over the infinite continuum states for shake-off. However, the determination of capture probabilities only requires the total probability $P_{m\kappa}$ of creating a secondary vacancy in an orbital (m, κ) consecutive to the capture of an electron in an orbital (n, κ) . Such a probability is simpler to calculate when considering the non-shaking probability, and can be expressed as [21]

$$P_{m\kappa} = 1 - \langle (m, \kappa)' | (m, \kappa) \rangle^{2n_{m\kappa}} - \sum_{l \neq m} \langle (l, \kappa)' | (m, \kappa) \rangle^2. \quad (5)$$

These effects are already taken into account in Bahcall modeling of overlap and exchange with the use of the closure property. On the contrary, they are not included in Vatai's approach. The shaking correction is therefore only applied along with Vatai modeling.

Finally, the possibility of radiative capture process is taken into account with radiative corrections, for which calculation depends on the atomic energies. However, they are only significant when a β^+ transition competes, i.e. for the determination of capture-to-positron ratios.

B. BetaShape wave functions

The relativistic electron wave functions in BetaShape are determined following essentially the method of Behrens and Bühring [18], as described in detail in [14,22]. A neutral atom is considered, which orbitals are filled in following the Madelung rule. The Coulomb potential of the nucleus is modeled from a uniformly charged sphere and a screened potential parameterized on Dirac-Hartree-Fock-Slater self-consistent results from [23]. For the bound states, an exchange potential is added that includes a constant prefactor. This prefactor is adjusted in order to force the convergence procedure to tabulated atomic energies.

As underlined by Vatai in [20], the vacancy created in a subshell by the capture process has a significant influence on all the orbitals. This hole effect is corrected employing first-order time-independent perturbation theory [15], as proposed by Vatai.

The tabulated atomic energies from Desclaux [24] for relativistic single electrons were used in a first study [15]. However, comparison with a selection of experimental values showed that the accuracy of the atomic wave functions was not sufficient to distinguish between Bahcall and Vatai models of overlap and exchange correction. In a second study [14], atomic energies from Kotochigova et al. [25] recommended on the NIST website [26] were considered. They had been determined for a point charge nucleus using the relativistic local-density approximation, including some electron correlations. Good agreement was found with experimental values and as expected, Vatai model of overlap and exchange, corrected for shaking, was found to be more accurate than Bahcall model.

It is clear that this method for determining the atomic wave functions is inconsistent: first, because the nucleus is a spherical charge distribution while Kotochigova's modeling is for a point charge nucleus; second, because no correlations are present in the adjusted Coulomb potential. On the contrary, the model described below is totally consistent. A specific version of the BetaShape code has been developed for using its wave functions as input, read from external files together with the energies and electronic configuration. The approximate correction of the hole effect has been removed and this effect is exactly taken into account by determining the wave functions for an electronic configuration with a vacancy due to capture.

C. A realistic atomic modeling

In order to describe the electron capture process, one has to work in the framework of relativistic quantum mechanics for describing the electronic part of the atom. In this context, it is also mandatory to include correlation effects – beyond mean-field – and nuclear finite size effects by using a precise description of the nucleus charge distribution – beyond the usual point charge approximation. Indeed, the penetration of the electron wave function inside the nucleus can be important for heavy elements.

One of the most popular and powerful method for including correlation effects at a rela-

tivistic level is the multiconfiguration Dirac-Fock (MCDF) model, which uses a linear combination of Slater determinants to approximate the electron many-body wave function [27]. However, due to the exponential increase with the atomic number of configurations involved in the computation, the use of MCDF is restricted to atoms having a relatively low atomic number ($Z < 30$).

An alternative approach, although a priori less accurate, is provided by the relativistic density functional theory (RDFT) within the local density approximation (RLDA) [28]. The latter is much less time consuming, more easy to use and able to cover a large number of radionuclides. In the present work, we have developed a specific calculation code based on this method. The main ingredients of RLDA are reminded below and we refer to [29,30,31] for more details. In the following, a spherical symmetry is assumed and atomic units are used if not otherwise stated.

In RDFT, one must solve the one electron Dirac equation

$$[T + \beta/\alpha^2 + V_{\text{eff}}[\rho](r)] \Psi_i(\vec{r}) = \varepsilon_i \Psi_i(\vec{r}) , \quad (6)$$

which can be expressed as

$$[\vec{\alpha} \cdot \vec{p}/\alpha + \beta/\alpha^2 + V_{\text{eff}}[\rho](r)] \Psi_i(\vec{r}) = \varepsilon_i \Psi_i(\vec{r}) , \quad (7)$$

where $\vec{\alpha}$ and β are the Dirac matrices [32], α is the fine structure constant, Ψ_i is a bi-spinor and $V_{\text{eff}}[\rho]$ is an effective spherical one-particle potential. T is the kinetic energy that introduces a coupling between the small and large components of the Dirac wave function and β/α^2 is the electron rest energy. The electron density is given by

$$\rho(r) = \sum_{i=1}^{N_{\text{orb}}} \Psi_i^\dagger(\vec{r}) \Psi_i(\vec{r}) = \sum_{i=1}^{N_{\text{orb}}} \rho_i(r) , \quad (8)$$

where N_{orb} is the number of orbitals.

Within the framework of RLDA, the effective potential can be expressed as

$$V_{\text{eff}}[\rho](r) = V_{\text{H}}[\rho](r) + V_{\text{xc}}[\rho](r) + V_{\text{ext}}(r) , \quad (9)$$

where $V_{\text{H}}[\rho](r) = \int \frac{\rho(r')}{|\vec{r} - \vec{r}'|} d\vec{r}'$ is the Hartree potential, $V_{\text{xc}}[\rho]$ is the relativistic exchange and correlation potential, and V_{ext} is the external potential due to the interaction of the electrons with the nucleus.

The nuclear charge distribution $\rho_{\text{nuc}}(r)$ is modeled by using a two-parameter Fermi-type distribution [33]. The value of the root mean square charge (RMS) radius of the nucleus, which is needed as an input parameter, is taken from [34] where existing experimental data are quoted. Otherwise, the empirical formula from [35] is used. The external potential V_{ext} is then computed thanks to

$$V_{\text{ext}}(r) = - \int \frac{\rho_{\text{nuc}}(r')}{|\vec{r} - \vec{r}'|} d\vec{r}' . \quad (10)$$

For $V_{\text{xc}}[\rho]$, we have used different exchange-correlation functionals: Vosko, Wilk and Nusair (VWN) [36], Gunnarsson and Lundqvist (GL) [37] and Perdew and Wang (PW) [38]. We have also implemented the gradient-dependent exchange-correlation functional of van Leeuwen and Baerends (LB) [39]. This functional is non-local and depends not only on the electron density but also on the electron density gradient.

We have elaborated a computer code for generating electron energies and wave functions. It is based on the numerical schemes of [40] and is complemented by the incorporation of a realistic description of the nucleus and by the implementation of the optimized effective potential method (see Section II D). We have used an exponential grid well adapted for radius values within the area of the nucleus, which are essential for the modeling of the electron capture process. The possibility to create atomic vacancies, as needed for the modeling of electron capture, has been also implemented.

D. Optimization of the effective potential

We have first tested and benchmarked our code by reproducing the atomic energies from Kotochigova et al. [25] for atoms from Hydrogen to Uranium. They have been obtained within the framework of RLDA using the Vosko, Wilk and Nusair exchange-correlation functional and a point charge model for describing the charge distribution of the nucleus.

In a second step, we have optimized our modeling in regards to the effective potential. For a neutral atom, the asymptotic behavior of the effective potential is given by the exchange contribution to V_{xc} , which behaves at large distance as $\rho^{1/3}$. As a consequence, the effective potential V_{eff} decreases exponentially to zero and does not reproduce the expected $1/r$ asymptotic behavior. This problem does not appear in the Dirac-Fock theory because the Dirac-Fock exchange potential exactly compensates the self-interaction term contained in the Hartree potential (see Figure 1).

Generally, the use of this correction leads to a much better description of the outermost shells. In particular, the experimental ionization potential can be generally well reproduced [39]. In addition, although it has not been studied in the present work, this correction is crucial for a correct description of unoccupied and continuum states that are essential for shake-up and shake-off processes. However, the drawback of this correction and its variants (ADSIC [41], SIC [42], GAM [43]) is an inaccurate description of the inner shells, which are mainly involved in the electron capture process (i.e. $1s_{1/2}$, $2s_{1/2}$, $2p_{1/2}$). A way to overcome this inconvenience is to use the optimized effective potential method, which was originally described within a non-relativistic framework by J. B. Krieger et al. [44,45] and extended to the relativistic case by Xiao-Min Tong and Shih-I Chu [46].

In order to compute the optimized effective potential $V_{\text{eff}}^{\text{KLI}}$ – giving what we call the KLI model in the following, one has to solved self-consistently the equation

$$\begin{aligned}
 V_{\text{eff}}^{\text{KLI}}(r) = & V_{\text{eff}}[\rho](r) + \frac{fo(N_{\text{orb}})\rho_{N_{\text{orb}}}(r)}{\rho(r)} \times (-V_{\text{H}}[\rho_{N_{\text{orb}}}] (r) - V_{\text{xc}}[\rho_{N_{\text{orb}}}] (r)) \\
 & + \sum_{i=1}^{N_{\text{orb}}-1} \frac{fo(i)\rho_i(r)}{\rho(r)} \times \{-V_{\text{H}}[\rho_i](r) - V_{\text{xc}}[\rho_i](r) \\
 & - \int_0^\infty \rho_i(r)(-V_{\text{xc}}[\rho_i](r) - V_{\text{H}}[\rho_i](r))r^2 dr + \int_0^\infty \rho_i(r)V_{\text{eff}}^{\text{KLI}}(r)r^2 dr\} ,
 \end{aligned} \tag{11}$$

where $fo(i)$ is the occupation number of the orbital i . The term $V_{\text{eff}}^{\text{KLI}}(r)$ that appears on both sides of the above equation will be quickly adjusted after a few iterations. All the details concerning the derivation of this equation are given in [46].

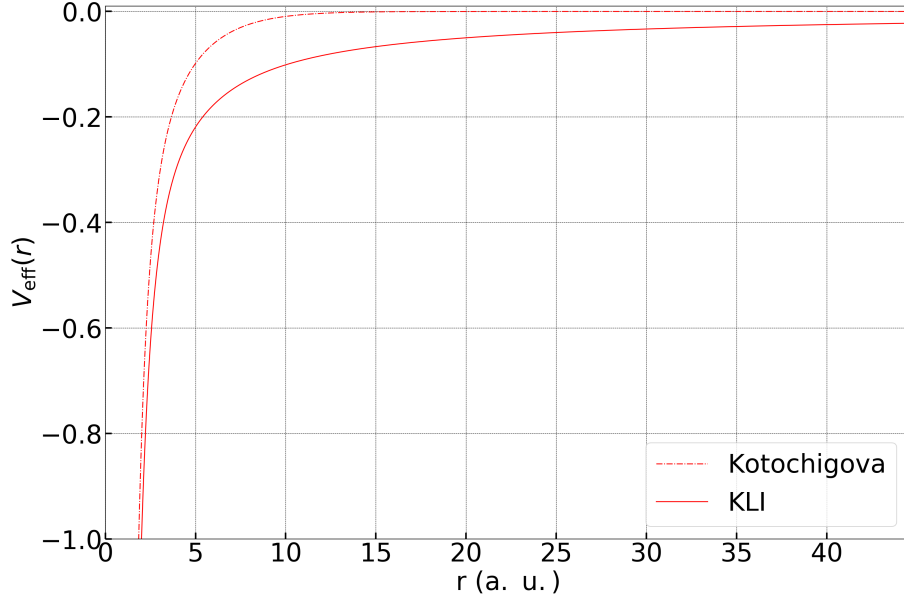


FIG. 1: (Color online) KLI (solid) and Kotochigova (dashed) effective potentials for ^{109}Cd .

III. Results

We have carried out many simulations employing different exchange-correlation functionals (VWN, GL, PW and LB) and self-interaction-corrected models (ADSIC, SIC, GAM and KLI). It turns out that KLI is the best compromise for obtaining: *i*) electron binding energies of inner subshells close to the experimental values (see Table I); and *ii*) a long-range Coulomb behavior of the effective potential (see Figure 1). Moreover, we have found that within the KLI model, the results depend only very slightly on the exchange-correlation functional utilized. Therefore, we have employed the VWN functional for the comparison of the results obtained with both Kotochigova and KLI models.

TABLE I: Binding energies (in atomic units) of the innermost orbitals for Kotochigova and KLI models. Experimental values have been taken in [47] for ^7Be and all values with uncertainties, and in [48] in other cases.

Element	1s			2s			2p _{1/2}		
	Koto.	KLI	Exp.	Koto.	KLI	Exp.	Koto.	KLI	Exp.
^7Be	-3.856	-4.815	-4.384	-0.206	-0.377	-0.343	–	–	–
^{41}Ca	-144.40	-148.93	-148.57 (7)	-15.16	-16.14	-16.26 (7)	-12.375	-13.394	-13.230 (4)
^{54}Mn	-235.08	-240.81	-240.70 (6)	-27.22	-28.38	-28.72 (6)	-23.368	-24.606	-24.357 (37)
^{55}Fe	-255.90	-261.88	-261.80 (4)	-29.99	-31.20	-31.49 (7)	-25.92	-27.21	-26.94 (4)
^{109}Cd	-968.69	-981.42	-981.60	-143.97	-146.64	-147.66	-23.37	-24.61	-24.36 (4)
^{125}I	-1204.13	-1218.71	-1218.93	-186.24	-189.33	-190.65	-174.98	-178.32	-178.31
^{138}La	-1414.24	-1430.37	-1430.46	-225.36	-228.79	-230.27	-212.81	-216.51	-216.49

A. Binding energies

Binding energies of the inner subshells of the atoms considered in this work are given in Table I for Kotochigova and KLI models, and are compared to experimental values taken in [47,48]. It is clear that KLI energies are much more accurate, which validates the approach developed to correct for the asymptotic behavior of the effective potential and to obtain accurate binding energies for the inner subshells.

B. Wave functions

The use of the KLI wave functions in the electron capture modeling described in Section II A requires, of course, to go from the atomic to the relativistic units. However, one also has to determine the Coulomb amplitudes $\beta_{n\kappa}$ for each wave function. In Behrens and Bühring formalism [18], the relativistic electron wave function is defined as

$$\psi_{n\kappa}(\vec{r}) = \begin{pmatrix} S_\kappa f_{n\kappa}(r) \chi_{-\kappa}^\mu \\ g_{n\kappa}(r) \chi_\kappa^\mu \end{pmatrix}, \quad (12)$$

where $f_{n\kappa}(r)$ and $g_{n\kappa}(r)$ are respectively the small and large radial components, and S_κ is the sign of κ . The usual spin-angular functions χ_κ^μ are defined on an orthonormal basis of spherical harmonics and are not of direct interest for the present work.

To compute these wave functions, Behrens and Bühring express the effective potential as a Taylor series

$$V_{\text{eff}} = \sum_{m=0}^{\infty} v_m r^m \quad (13)$$

and introduce a local power series expansion that gives close to the origin

$$\begin{Bmatrix} f_{n\kappa}(r) \\ g_{n\kappa}(r) \end{Bmatrix} = \beta_{n\kappa} \frac{(p_{n\kappa} r)^{k-1}}{(2k-1)!!} \sum_{j=0}^{\infty} \begin{Bmatrix} a_j \\ b_j \end{Bmatrix} r^j. \quad (14)$$

The series coefficients are defined by the following recurrence relationships:

$$\begin{aligned} a_0 &= 1, & b_0 &= 0 \text{ if } \kappa > 0 \\ a_0 &= 0, & b_0 &= 1 \text{ if } \kappa < 0 \end{aligned} \quad (15)$$

and

$$\begin{aligned} (j+k-\kappa)a_j &= -(W-1-v_0)b_{j-1} + \sum_{m=1}^{j-1} v_m b_{n-m-1} \\ (j+k+\kappa)b_j &= (W+1-v_0)a_{j-1} - \sum_{m=1}^{j-1} v_m a_{n-m-1} \end{aligned} \quad (16)$$

with W the total energy of the electron.

The effective KLI potential is locally fitted, after convergence, with a third order polynomial. The determination of the Coulomb amplitude $\beta_{n\kappa}$ is then straightforward knowing the radial wave functions. In Table II, we compare some Coulomb amplitudes for different atoms determined with BetaShape, Kotochigova and KLI models. As explained below, the differences are due to the binding energies and the nucleus modeling.

We present in Figure 2 a comparison of the $1s$ and $2s$ wave functions in neutral ${}^7\text{Be}$ ($Z = 4$) for the three different atomic models considered in this work. As expected for

TABLE II: Coulomb amplitudes $\beta_{n\kappa}$ for different atoms considered in the present work. The electronic configuration corresponds to neutral, fully relaxed atoms.

Element	β_{1s}			β_{2s}			$\beta_{2p_{1/2}}$		
	BS	Koto.	KLI	BS	Koto.	KLI	BS	Koto.	KLI
^7Be	0.008763	0.009073	0.009295	0.001584	0.001862	0.002110	–	–	–
^{41}Ca	0.1174	0.1186	0.1174	0.03324	0.03449	0.03417	0.001823	0.001879	0.001929
^{54}Mn	0.1690	0.1742	0.1707	0.05263	0.05299	0.05200	0.003756	0.003743	0.003775
^{55}Fe	0.1806	0.1867	0.1825	0.05665	0.05721	0.05601	0.004225	0.004227	0.004249
^{109}Cd	0.5825	0.6414	0.5830	0.1955	0.2180	0.1983	0.02898	0.03214	0.02971
^{125}I	0.7224	0.8161	0.7248	0.2507	0.2829	0.2514	0.04140	0.04668	0.04213
^{138}La	0.8576	0.9864	0.8585	0.2985	0.3474	0.3025	0.05382	0.06231	0.05509

low- Z atoms, relativistic effects are very weak, leading to $f \ll g$. We can also expect that the finite size of the nucleus should play a minor role. It is indeed the case since the large component g of the wave function exhibits the same behavior in the three models. Concerning the small component f (which is approximately 100 times smaller), a different behavior can be seen between the wave function from Kotochigova model and those from KLI and BetaShape. It shows up within the area of the nucleus. This difference is due to the modeling of the nucleus charge distribution in the three models: point charge for Kotochigova, sphere with uniform charge density for BetaShape and Fermi distribution for KLI.

Similarly, we present in Figure 3 the same comparison for neutral ^{138}La ($Z = 57$). As expected for medium- Z atoms, relativistic effects start to become important leading to a non-negligible small component $f < g$. With respect to the case of ^7Be , the difference between the binding energies ($1s$ and $2s$) of Kotochigova (also used in BetaShape) and KLI is relatively much smaller (see Table I). Consequently, one also expect a smaller difference between the wave functions, what can clearly be seen on Figure 3 for distances greater than the nuclear radius (1.6×10^{-2} rel. u.). For smaller distances, the wave functions from Kotochigova model and those from KLI and BetaShape differ, here again, due to the different modeling of the nuclear charge distribution.

In order to see more differences between BetaShape and KLI models, let us now investigate the higher $2p_{1/2}$ and $5s$ orbitals, for which wave functions are presented in Figure 4. The analysis of $2p_{1/2}$ is similar to the one given for $1s$ or $2s$. For the $5s$ orbital, relatively large differences can be observed. This tendency is certainly due to the large difference (13%) between the binding energies: 38.924 eV for Kotochigova and BetaShape, and 44.115 eV for KLI. The choice of $5s$ was motivated by the fact that this outer s orbital has a non-negligible probability of presence inside the nucleus.

C. Capture probabilities

Internal conversion theory has been recently tested comparing precise measurements with different predictions [49]. Two hypotheses were considered: *i*) the “no vacancy” approximation, which assumes a final state corresponding to the daughter atom after full atomic

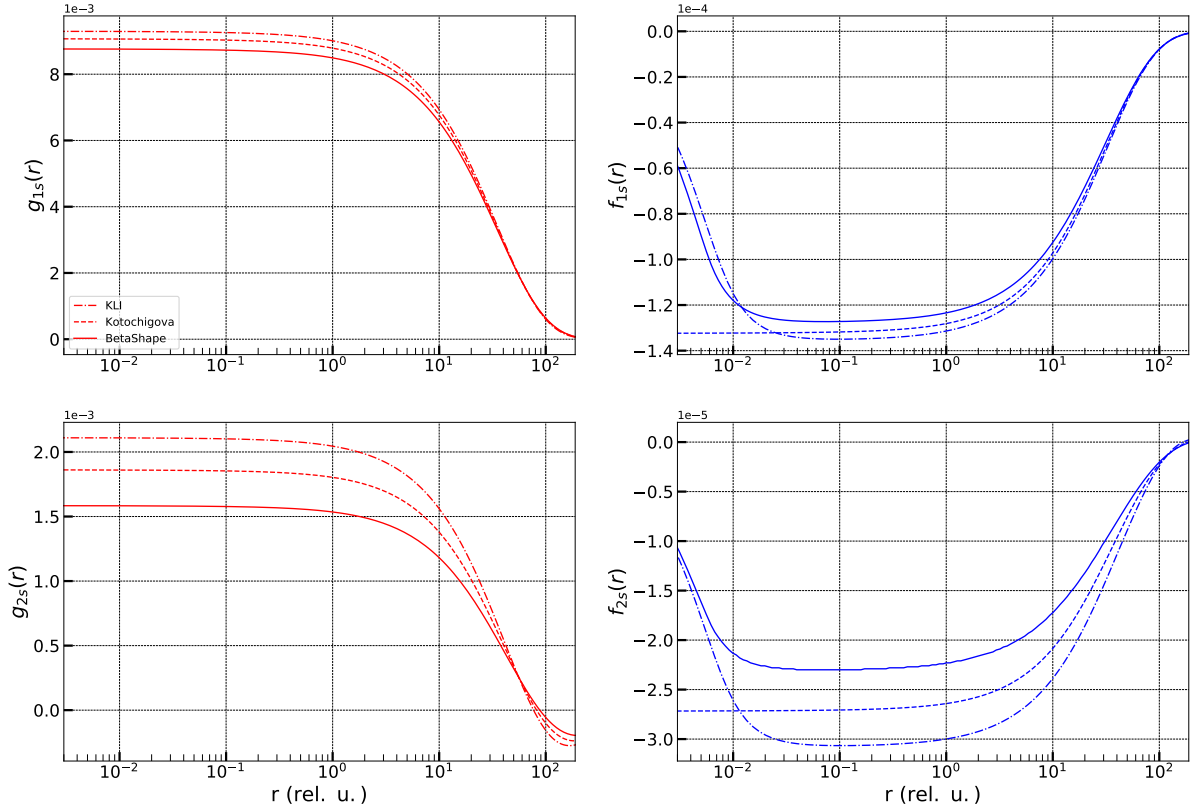


FIG. 2: (Color online) Large (g) and small components (f) of the radial wave functions for the $1s$ and $2s$ orbitals of ${}^7\text{Be}$. Dash-dotted, dashed and solid curves are from KLI, Kotochigova and BetaShape models, respectively.

relaxation; and *ii*) the “frozen orbital” (FO) approximation, which assumes that the final atomic orbitals in the internal conversion process correspond to those of the parent atom with a vacancy. It was found that FO approximation gives the most accurate and consistent results over a wide range of atomic numbers, as expected from the time scales of the physical processes [50].

The situation is comparable for electron capture. The weak interaction transforms the parent nucleus with atomic number Z into the daughter nucleus with atomic number $(Z - 1)$. This interaction is mediated by massive bosons and is therefore of very short range. The time scale of the electron capture decay might thus be seen as instantaneous compared to the atomic time scale, i.e. the vacancy lifetime. The BetaShape modeling assumes the FO approximation, and we have considered with the KLI modeling both the FO and the “no vacancy” approximations. We underline that in the latter case, the hole effect is obviously not taken into account.

The dominant electron capture transition in each of the radionuclides of interest for the European project MetroMMC have been studied. Calculation of capture probabilities have been performed using the recommended Q-values established in the latest Atomic Mass Evaluation AME2020 [51]. Nuclear level energies have been taken from the latest ENSDF evaluations for the following decays: ${}^{54}\text{Mn}$ [52], ${}^{109}\text{Cd}$ [53], ${}^{125}\text{I}$ [54] and ${}^{138}\text{La}$ [55]. The results are given in Table III together with experimental values when available and are discussed below.

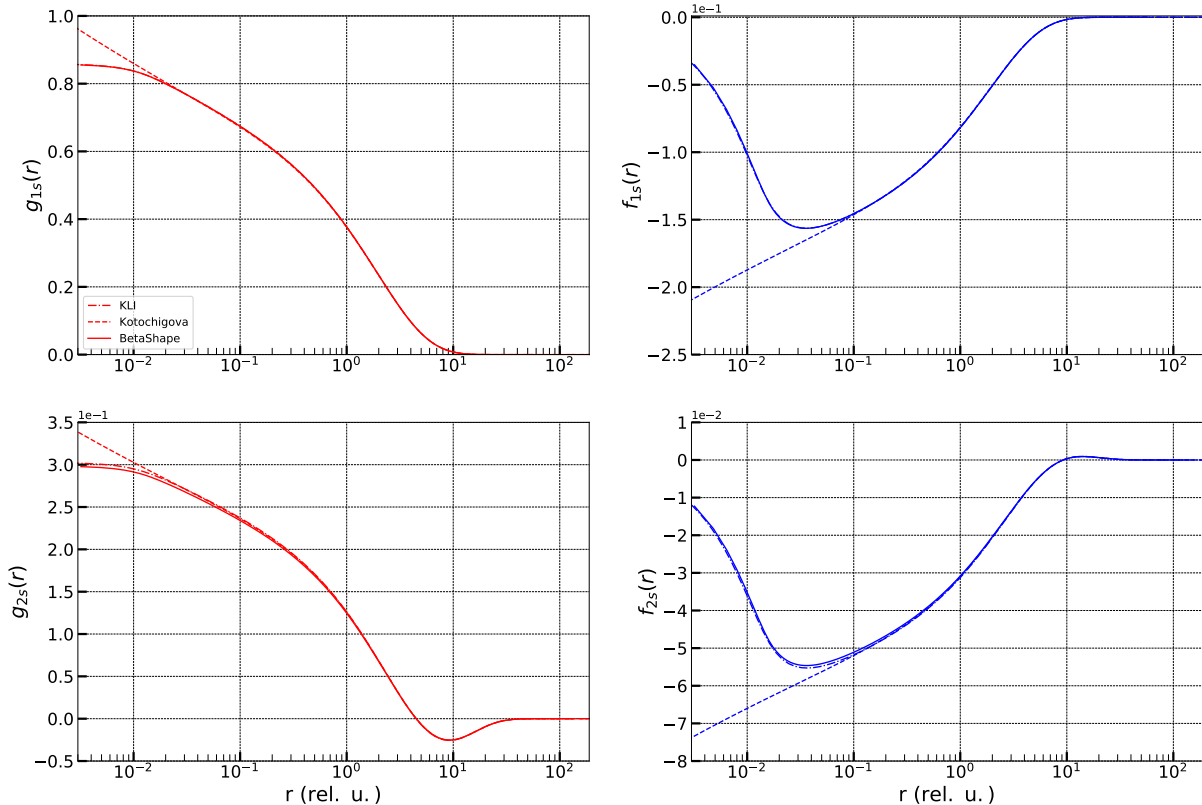


FIG. 3: (Color online) Large (g) and small components (f) of the radial wave functions for the $1s$ and $2s$ orbitals of ^{138}La . Dash-dotted, dashed and solid curves are from KLI, Kotochigova and BetaShape models, respectively.

^7Be . This decay has been measured a lot for decades. Its chemical form has been demonstrated to have a significant influence on the half-life, which seems reasonable with such a small number of atomic orbitals. The P_L/P_K ratio is thus expected to be influenced by environmental effects. The experimental value is from a precise measurement in which ^7Be was implanted in a thin Ta metallic film [56]. It is clear that none of the calculated values agrees and that the atomic modeling has a very strong impact on the P_L/P_K ratio, with a factor of 2 to 3 between the predictions. It is noteworthy that such a difference appears only for this radionuclide. The difference with the experimental value could be due in part to the assumption of a decay in vacuum. In medium effects were estimated in [57] and, if this simple modeling is correct, a strong correction factor of 0.2986 is expected for metallic Ta. Applying this correction to our predictions does not help to agree with the experimental value.

^{41}Ca . To our knowledge, no experimental value of any capture probability is available in the literature for this radionuclide. We can simply observe that the BetaShape value lies in between the “no vacancy” and the FO KLI results, and that the FO approximation tends to decrease the P_L/P_K ratio.

^{54}Mn . The first experimental value comes from the weighted mean of two old measurements with quite large uncertainties: $P_L/P_K = 0.098$ (6) from [58] and $P_L/P_K = 0.106$ (3) from [59]. Even if the “no vacancy” KLI result seems to be the best prediction, it is difficult to be conclusive.

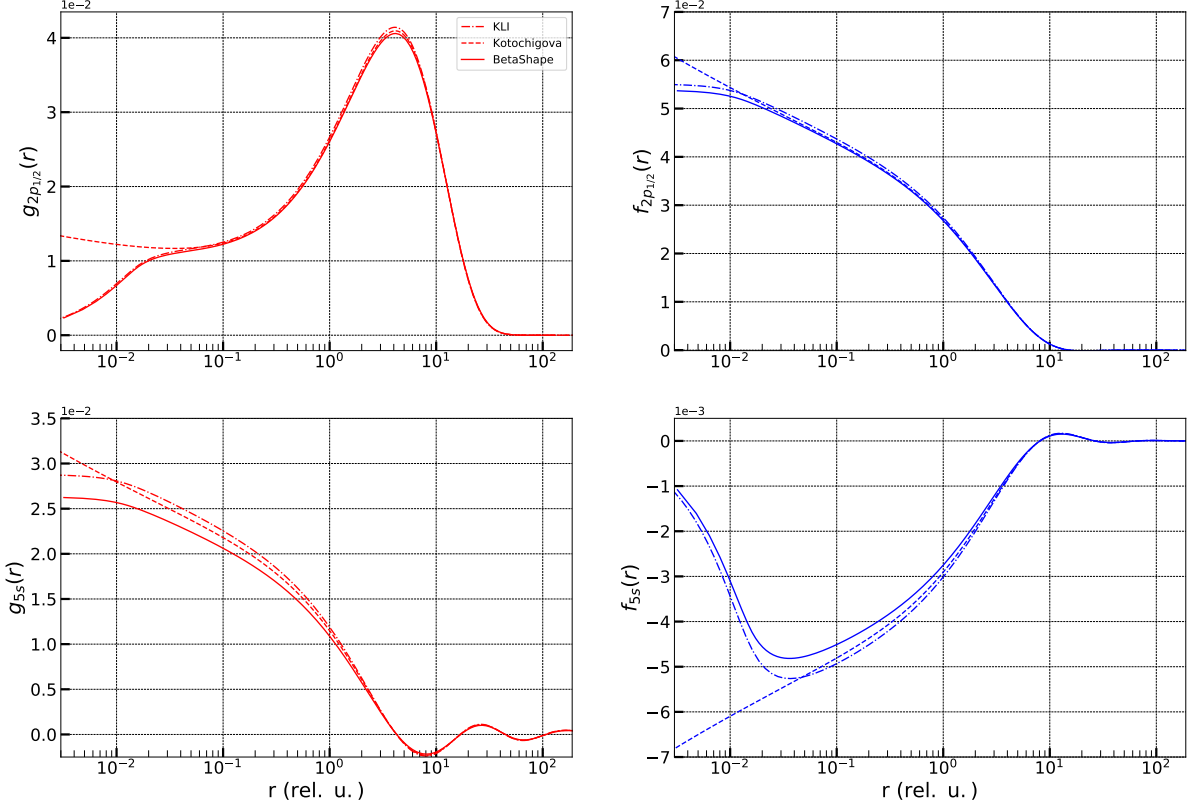


FIG. 4: (Color online) Large (g) and small components (f) of the radial wave functions for the $2p_{1/2}$ and $5s$ orbital of ^{138}La . Dash-dotted, dashed and solid curves are from KLI, Kotochigova and BetaShape models, respectively.

The experimental P_K probability has been determined with measured values listed in [17] and complemented with those in the DDEP evaluation [60]. Only two measurements, consistent, do not depend on the fluorescence yield ω_K and their weighted mean is $P_K = 0.901$ (6). Nine other measurements do depend on ω_K . The resulting dataset being discrepant, the uncertainty on their weighted mean has been expanded in order to include the most precise value, leading to $P_K\omega_K = 0.253$ (6). It is interesting to note that the fluorescence yield used in the DDEP evaluation from a semi-empirical fit from Bambynek [61], $\omega_K = 0.289$ (5), is significantly different to the older experimental value from the same author [62], $\omega_K = 0.2793$ (17). With the former, one obtains a value of $P_K = 0.875$ (26) while with the latter, one has the higher value $P_K = 0.906$ (22). Comparing with the first result, it suggests that the correct fluorescence yield is the experimental value, and we have chosen for our comparison the most precise P_K value. The FO KLI prediction is in very good agreement, which is definitely not the case for the other two theoretical results.

^{55}Fe . All three experimental capture probability ratios result from the weighted means of two precise measurements [63,64]. Surprisingly, the BetaShape predictions exhibit excellent agreement for the P_L/P_K and P_M/P_L ratios while calculations performed with the KLI atomic modeling not. It is noteworthy that the three capture ratios are not consistent. Calculating P_M/P_K from the weighted means of the other two, one find a significantly higher value of $P_M/P_K = 0.01813$ (33), which is again in excellent agreement with the BetaShape result but with none of the KLI predictions.

TABLE III: Comparison of calculated and measured capture probabilities for the different isotopes considered in the present work. The three models and the experimental values are described in the text.

Isotope	Energy (keV)	Quantity	BetaShape	KLI		Experimental
				“no vacancy”	“frozen orbital”	
⁷ Be	861.89 (7)	P_L/P_K	0.105 (8)	0.1606 (41)	0.0509 (20)	0.070 (7)
⁴¹ Ca	421.64 (14)	P_L/P_K	0.09800 (40)	0.10415 (16)	0.09078 (16)	–
⁵⁴ Mn	542.2 (10)	P_L/P_K	0.11219 (31)	0.10785 (8)	0.09590 (19)	0.1044 (27)
		P_K	0.88419 (34)	0.88623 (10)	0.90005 (21)	0.901 (6)
⁵⁵ Fe	231.12 (18)	P_L/P_K	0.11629 (31)	0.11236 (8)	0.10073 (20)	0.1165 (9)
		P_M/P_K	0.01824 (12)	0.019390 (32)	0.014824 (45)	0.01786 (29)
		P_M/P_L	0.1568 (11)	0.17257 (31)	0.14716 (49)	0.1556 (26)
¹⁰⁹ Cd	127.1 (18)	P_K	0.8148 (14)	0.8097 (11)	0.8164 (12)	0.815 (2)
		P_{LMNO}/P_K	0.2274 (12)	0.2350 (11)	0.2250 (12)	0.2279 (21)
¹²⁵ I	150.28 (6)	P_K	0.79927 (41)	0.79798 (7)	0.80376 (23)	0.7971 (14)
¹³⁸ La	312.60 (30)	P_L/P_K	0.3913 (25)	0.4077 (15)	0.4242 (49)	0.391 (3)
		P_M/P_K	0.0965 (9)	0.09908 (41)	0.1002 (11)	0.102 (3)
		P_M/P_L	0.2465 (20)	0.2430 (22)	0.2362 (24)	0.261 (9)

¹⁰⁹Cd. The experimental values have been determined as weighted means of several measurements listed in [65]. The P_{LMNO}/P_K value has been reevaluated by revising one of the measured values as suggested in [17]. Both BetaShape and FO KLI predictions are in very good agreement with experiment, while the “no vacancy” KLI results are significantly not in accordance.

¹²⁵I. Seven measurements of the P_K capture probability were performed in the past, listed in [17,66]. The experimental value in Table III results from their weighted mean. The value is largely dominated by a single old measurement from [67] and only a slight dependency in the ω_K fluorescence yield is expected. For this radionuclide, the “no vacancy” KLI result is the only one being in good agreement, the other two models predicting a higher K capture probability.

¹³⁸La. This transition is the only one considered in the present study that is not allowed, being second forbidden unique. In this case, $C_{n\kappa}$ is not equal to unity and must be taken into account. All the measured values come from a single recent experiment [68]. The situation is quite unclear as it depends on the capture probability ratio that is considered. For P_L/P_K , the BetaShape result is in remarkable accordance with the experimental value. It is the contrary for P_M/P_K , KLI results being in excellent agreement with a slight advantage for the FO approximation. For P_M/P_L , no theoretical prediction agrees with the measurement.

However, as underlined in [68] ¹³⁸La decay seems to be sensitive to its particular nuclear structure and additional terms in $C_{n\kappa}$ might be necessary due to accidental cancellation of the dominant nuclear matrix element. In [14], the nuclear levels were described quite simply as single particle states and the BetaShape results were found to be in better agreement with the measured values.

IV. Conclusions and perspectives

For the past few years, the DDEP international collaboration has employed the BetaShape code in their evaluated nuclear decay data in order to improve the accuracy of the beta and electron capture properties. In the present work, we have performed an exhaustive study of the role played by the modeling of the atomic electrons on the electron capture process.

A realistic model has been developed within the framework of RDFT, in which we have implemented few exchange-correlation functionals and self-interaction-corrected models, among the most popular in the community. From our analysis, we found that the best choice which fulfills some physical constraints (binding energies of inner subshells, asymptotic behavior of the effective potential) is provided by the optimized effective potential method originally developed by Krieger, Li and Iafrate (KLI). It turns out that, within this model, correlation effects seem to play a minor role. However, a more precise study would be required in order to obtain a more decisive conclusion on that issue.

The electron capture model has been adapted in order to consistently use the binding energies, wave functions and electronic configurations from the KLI code. It allowed us to precisely include the hole effect on the other orbitals, due to the vacancy created by the capture process, while this effect is accounted for approximately with the BetaShape atomic modeling. We have demonstrated a posteriori why the latter modeling can lead to surprisingly good results. When Kotochigova and KLI binding energies are relatively close to each other, i.e. for the innermost shells, introducing a nucleus spatial extension instead of considering a point charge gives the dominant distortion on the radial wave functions close to the origin. However, it also seems that some inaccuracies (hole and shaking effects, which depend on the different possible overlaps) somehow compensate each other.

Several transitions of interest have been calculated and the theoretical capture probabilities have been compared to experimental values. Such a test covers a wide range of atomic numbers, $3 \leq Z \leq 57$. As in the early stage of the study of internal conversion [50], the situation is unclear and unsatisfactory and we face to similar difficulties. The KLI model with the “frozen orbital” approximation should in principle provide the most accurate predictions. Our analysis of the published experimental values has shown that new high-precision measurements are definitely required. It is also necessary to have a more complete set of measured capture probabilities for each transition because one or two are not sufficient to be conclusive, especially for the outer shells. One can expect that these new accurate experimental values and further improvements of the theoretical models will clarify the situation, as it did with internal conversion [49].

In the near future, the electron capture model should benefit from ongoing developments on beta decay that aim at including a realistic nuclear structure for the calculation of forbidden non-unique transitions. Such an improvement will necessitate a revision of the overlap and exchange correction, with a precise coupling of lepton and nucleon wave functions.

Within the framework of the KLI atomic model, efforts will be devoted to the separate computation of shake-up and shake-off processes. Indeed, good description of the unoccupied levels and the continuum states is mandatory for such processes, shake-off being in particular conditioned by the asymptotic behavior of the effective potential.

A more precise study devoted to the role played by the correlation effects on electron capture probabilities is also required. A comparison between the present results and those obtained with the MCDF method for light atoms (e.g. ${}^7\text{Be}$ and ${}^{41}\text{Ca}$) will be investigated, what could lead to a revised parameterization of the correlation potential.

Finally, another important issue concerns the role played by the environment on the

electron capture process, as it has been seen e.g. in ${}^7\text{Be}$ decay. Such a complicated problem deserves in itself a detailed specific study.

Acknowledgments

This work was performed within the European project MetroMMC, “Measurement of fundamental nuclear decay data using metallic magnetic calorimeters”. This project 17FUN02 MetroMMC has received funding from the EMPIR programme co-financed by the Participating States and from the European Union’s Horizon 2020 research and innovation programme.

-
- [1] R. Coulon, R. Broda, P. Cassette, S. Courte, S. Jerome, S. Judge, K. Kossert, H. Liu, C. Michotte, and M. Nonis, *Metrologia* **57**, 035009 (2020).
 - [2] R. Broda, P. Cassette, and K. Kossert, *Metrologia* **44**, S36 (2007).
 - [3] B. M. Bavelaar, B. Q. Lee, M. R. Gill, N. Falzone, and K. A. Vallis, *Frontiers in Pharmacology* **9**, 996 (2018).
 - [4] A. Ku, V. J. Facca, Z. Cai, and R. M. Reilly, *EJNMMI Radiopharmacy and Chemistry* **4**, 27 (2019).
 - [5] X. Hou, *Radiochimica Acta* **93**, 611 (2005).
 - [6] Y.-J. Lee, J.-M. Lim, J.-H. Lee, S.-B. Hong, and H. Kim, *Nuclear Engineering and Technology* **53**, 1210 (2021).
 - [7] G. R. Huss, B. S. Meyer, G. Srinivasan, J. N. Goswami, and S. Sahijpal, *Geochimica et Cosmochimica Acta* **73**, 4922 (2009).
 - [8] G. Jörg, Y. Amelin, K. Kossert, and C. Lierse v. Gostomski, *Geochimica et Cosmochimica Acta* **88**, 51 (2012).
 - [9] P. W. Kubik, D. Elmore, N. J. Conard, K. Nishiizumi, and J. R. Arnold, *Nature* **319**, 568 (1986).
 - [10] M. R. Bhat, in *Nuclear Data for Science and Technology*, edited by S. M. Qaim (Springer, Berlin, Heidelberg, 1992) pp. 817–821.
 - [11] Kellett, Mark A. and Bersillon, Olivier, *EPJ Web Conf.* **146**, 02009 (2017).
 - [12] N. Gove and M. Martin, *Atomic Data and Nuclear Data Tables* **10**, 205 (1971).
 - [13] X. Mougeot, *Phys. Rev. C* **91**, 055504 (2015).
 - [14] X. Mougeot, *Appl. Radiat. Isot.* **154**, 108884 (2019).
 - [15] X. Mougeot, *Appl. Radiat. Isot.* **134**, 225 (2018).
 - [16] P. C.-O. Ranitzsch, D. Arnold, J. Beyer, L. Bockhorn, J. J. Bonaparte, C. Enss, K. Kossert, S. Kempf, M. Loidl, R. Mariam, O. J. Nähle, M. Paulsen, M. Rodrigues, and M. Wegner, *Journal of Low Temperature Physics* **199**, 441 (2020).
 - [17] W. Bambynek, H. Behrens, M. H. Chen, B. Crasemann, M. L. Fitzpatrick, K. W. D. Ledingham, H. Genz, M. Mutterer, and R. L. Intemann, *Rev. Mod. Phys.* **49**, 77 (1977).
 - [18] H. Behrens and W. Bühring, *Electron Radial Wave Functions and Nuclear Beta Decay* (Clarendon, Oxford, 1982).
 - [19] J. N. Bahcall, *Nuclear Physics* **71**, 267 (1965).
 - [20] E. Vatai, *Nuclear Physics A* **156**, 541 (1970).

- [21] B. Crasemann, M. H. Chen, J. P. Briand, P. Chevallier, A. Chetioui, and M. Tavernier, *Phys. Rev. C* **19**, 1042 (1979).
- [22] X. Mougeot and C. Bisch, *Phys. Rev. A* **90**, 012501 (2014).
- [23] F. Salvat, J. D. Martínez, R. Mayol, and J. Parellada, *Phys. Rev. A* **36**, 467 (1987).
- [24] J. Desclaux, *Atomic Data and Nuclear Data Tables* **12**, 311 (1973).
- [25] S. Kotochigova, Z. H. Levine, E. L. Shirley, M. D. Stiles, and C. W. Clark, *Phys. Rev. A* **55**, 191 (1997).
- [26] S. Kotochigova, Z. H. Levine, E. L. Shirley, M. D. Stiles, and C. W. Clark, *NIST Chemistry WebBook, NIST Standard Reference Database 141*, edited by P. Linstrom and W. Mallard (National Institute of Standards and Technology, Gaithersburg MD, 20899, 2021) Chap. Atomic Reference Data for Electronic Structure Calculations.
- [27] J. Desclaux, *Computer Physics Communications* **9**, 31 (1975).
- [28] R. M. Dreizler and E. Engel, “Relativistic density functional theory,” in *Density Functionals: Theory and Applications: Proceedings of the Tenth Chris Engelbrecht Summer School in Theoretical Physics Held at Meerensee, near Cape Town South Africa, 19–29 January 1997*, edited by D. Joubert (Springer, Berlin, Heidelberg, 1998) pp. 147–189.
- [29] A. K. Rajagopal, *Journal of Physics C: Solid State Physics* **11**, L943 (1978).
- [30] A. H. MacDonald and S. H. Vosko, *Journal of Physics C: Solid State Physics* **12**, 2977 (1979).
- [31] E. Engel, *Relativistic Electronic Structure Theory, Part 1. Fundamentals*, edited by P. Schwerdtfeger (Elsevier, Amsterdam, 2002) pp. 524–624.
- [32] P. Strange, *Relativistic Quantum Mechanics: With Applications in Condensed Matter and Atomic Physics* (Cambridge University Press, 2008).
- [33] A. Pálffy, *Contemporary Physics* **51**, 471 (2010).
- [34] I. Angeli and K. Marinova, *Atomic Data and Nuclear Data Tables* **99**, 69 (2013).
- [35] W. Johnson and G. Soff, *Atomic Data and Nuclear Data Tables* **33**, 405 (1985).
- [36] S. H. Vosko, L. Wilk, and M. Nusair, *Canadian Journal of Physics* **58**, 1200 (1980).
- [37] O. Gunnarsson and B. I. Lundqvist, *Phys. Rev. B* **13**, 4274 (1976).
- [38] J. P. Perdew and Y. Wang, *Phys. Rev. B* **45**, 13244 (1992).
- [39] R. van Leeuwen and E. J. Baerends, *Phys. Rev. A* **49**, 2421 (1994).
- [40] O. Čertík, J. E. Pask, and J. Vackář, *Computer Physics Communications* **184**, 1777 (2013).
- [41] I. Ciofini, C. Adamo, and H. Chermette, *Chemical Physics* **309**, 67 (2005), electronic Structure Calculations for Understanding Surfaces and Molecules. In Honor of Notker Roesch.
- [42] J. P. Perdew and A. Zunger, *Phys. Rev. B* **23**, 5048 (1981).
- [43] M. F. Politis, P. A. Hervieux, J. Hanssen, M. E. Madjet, and F. Martín, *Phys. Rev. A* **58**, 367 (1998).
- [44] J. B. Krieger, Y. Li, and G. J. Iafrate, *Phys. Rev. A* **46**, 5453 (1992).
- [45] Y. Li, J. B. Krieger, and G. J. Iafrate, *Phys. Rev. A* **47**, 165 (1993).
- [46] X.-M. Tong and S.-I. Chu, *Phys. Rev. A* **57**, 855 (1998).
- [47] K. D. Sevier, *Atomic Data and Nuclear Data Tables* **24**, 323 (1979).
- [48] J. A. Bearden and A. F. Burr, *Rev. Mod. Phys.* **39**, 125 (1967).
- [49] J. Hardy, N. Nica, V. Iacob, and M. Trzhaskovskaya, *Applied Radiation and Isotopes* **134**, 406 (2018).
- [50] J. Hardy, N. Nica, V. Iacob, S. Miller, M. Maguire, and M. Trzhaskovskaya, *Applied Radiation and Isotopes* **87**, 87 (2014).
- [51] M. Wang, W. Huang, F. Kondev, G. Audi, and S. Naimi, *Chinese Physics C* **45**, 030003 (2021).

- [52] Y. Dong and H. Junde, Nuclear Data Sheets **121**, 1 (2014).
- [53] S. Kumar, J. Chen, and F. Kondev, Nuclear Data Sheets **137**, 1 (2016).
- [54] J. Katakura, Nuclear Data Sheets **112**, 495 (2011).
- [55] J. Chen, Nuclear Data Sheets **146**, 1 (2017).
- [56] S. Fretwell, K. G. Leach, C. Bray, G. B. Kim, J. Dilling, A. Lennarz, X. Mougeot, F. Ponce, C. Ruiz, J. Stackhouse, and S. Friedrich, Phys. Rev. Lett. **125**, 032701 (2020).
- [57] A. Ray, P. Das, S. K. Saha, S. K. Das, and A. Mookerjee, Phys. Rev. C **66**, 012501 (2002).
- [58] R. B. Moler and R. W. Fink, Phys. Rev. **131**, 821 (1963).
- [59] G. Manduchi and G. Zannoni, Il Nuovo Cimento **27**, 251 (1963).
- [60] M.-M. Bé, V. Chisté, C. Dulieu, E. Browne, V. Chechev, N. Kuzmenko, R. Helmer, A. Nichols, E. Schönfeld, and R. Dersch, *Table of Radionuclides*, Monographie BIPM-5, Vol. 1 (Bureau International des Poids et Mesures, Pavillon de Breteuil, F-92310 Sèvres, France, 2004) ; Evaluation update in 2014.
- [61] W. Bambynek, in *X-84 Proc. X-ray and Inner-Shell Processes in Atoms, Molecules and Solids, Leipzig Aug. 20-23, 1984*, edited by A. Meisel (VEB Druckerei, Thomas Münzer, Langensalza, 1984) post-deadline paper P-1.
- [62] W. Bambynek, Zeitschrift für Physik **206**, 66 (1967).
- [63] J. G. Pengra, H. Genz, J. P. Renier, and R. W. Fink, Phys. Rev. C **5**, 2007 (1972).
- [64] M. Loidl, M. Rodrigues, and R. Mariam, Applied Radiation and Isotopes **134**, 395 (2018).
- [65] M.-M. Bé, V. Chisté, C. Dulieu, M. Kellett, X. Mougeot, A. Arinc, V. Chechev, N. Kuzmenko, T. Kibédi, A. Luca, and A. Nichols, *Table of Radionuclides*, Monographie BIPM-5, Vol. 8 (Bureau International des Poids et Mesures, Pavillon de Breteuil, F-92310 Sèvres, France, 2016).
- [66] M.-M. Bé, V. Chisté, C. Dulieu, X. Mougeot, V. Chechev, N. Kuzmenko, F. Kondev, A. Luca, M. Galán, A. Nichols, A. Arinc, A. Pearce, X. Huang, and B. Wang, *Table of Radionuclides*, Monographie BIPM-5, Vol. 6 (Bureau International des Poids et Mesures, Pavillon de Breteuil, F-92310 Sèvres, France, 2011).
- [67] H. Leutz and K. Ziegler, Nuclear Physics **50**, 648 (1964).
- [68] F. Quarati, P. Dorenbos, and X. Mougeot, Applied Radiation and Isotopes **109**, 172 (2016).